Probing Hot Spots at Protein−Ligand Binding Sites: A Fragment-Based Approach Using Biophysical Methods

Alessio Ciulli,[†] Glyn Williams,[‡] Alison G. Smith,[§] Tom L. Blundell,[||] and Chris Abell*,[†]

University Chemical Laboratory, University of Cambridge, Lensfield Road, Cambridge CB2 1EW, Astex Therapeutics Ltd., 436 Cambridge Science Park, Milton Road, Cambridge CB4 0QA, Department of Plant Sciences, University of Cambridge, Downing Street, Cambridge CB2 3EA, and Department of Biochemistry, University of Cambridge, 80 Tennis Court Road, Cambridge CB2 1GA, United Kingdom

Received April 26, 2006

Mapping interactions at protein−ligand binding sites is an important aspect of understanding many biological reactions and a key part of drug design. In this paper, we have used a fragment-based approach to probe "hot spots" at the cofactor-binding site of a model dehydrogenase, *Escherichia coli* ketopantoate reductase. Our strategy involved the breaking down of NADPH (K_d = 300 nM) into smaller fragments and the biophysical characterization of their binding using WaterLOGSY NMR spectroscopy, isothermal titration calorimetry (ITC), and inhibition studies. The weak binding affinities of fragments were measured by direct ITC titrations under low *c* value conditions. The 2′-phosphate and the reduced nicotinamide groups were found to contribute a large part of the binding energy. A combination of ITC and site-directed mutagenesis enabled us to locate the fragments at separate hot spots on opposite ends of the cofactor-binding site. This study has identified structural determinants for cofactor recognition that represent a blueprint for future inhibitor design.

Introduction

The identification of potential ligand-binding sites on a target protein is fundamental for successful inhibitor design. Intriguingly, it has been recognized that for many protein complexes only relatively small regions of the binding surface, often called "hot spots", contribute a major part of the binding energy.[1−3] Within this context, Fesik and co-workers have recently analyzed the relationships between the ability of small molecules to bind to a protein and various physical parameters that describe the protein binding site.[4] It was found that small organic compounds bind almost exclusively to well-defined, localized regions of proteins, independent of their affinity. Once these hot spots are identified, binding interactions with adjacent regions of the protein surface can be subsequently explored to increase selectivity and improve affinity.[5]

In this study, we have used a fragment-based approach to identify hot spots at an enzyme active site using biophysical methods. Fragment-based approaches have recently emerged as attractive alternatives to high-throughput screening for drug design. They rely on the identification of low-molecular-weight compounds that bind to the target protein and are much smaller and functionally simpler than drugs.[6,7] Although affinities of bound fragments are low, a high proportion of their atoms make favorable contacts with the protein, and key interactions are formed.[8−10] As a result, fragments can be highly efficient ligands that preferentially fill hot spots on the protein surface.[4,5] Biophysical techniques such as NMR spectroscopy, X-ray crystallography, mass spectrometry, and isothermal titration calorimetry (ITC)[a] are particularly amenable to detect low-affinity binding and thus are ideal for fragment identification and characterization.[11−14] Furthermore, detection of binding is often direct and does not require labeling of the ligand or the protein, thereby minimizing false positives due to nonspecific associations as well as false negatives.[15,16] Although their implementation as high-throughput methods for compound screening can be costly or not practical in many cases, biophysical methods are now being developed as lead discovery tools.[17,18]

Here we have used *Escherichia coli* ketopantoate reductase (KPR; EC 1.1.1.169) as a model system to probe hot spots for ligand binding. KPR catalyzes the reduction of ketopantoate to form pantoate using NADPH as a cofactor (Scheme 1) in the biosynthetic pathway leading to pantothenate (vitamin B5), the key precursor for coenzyme A.[11,19] The absence of this enzyme in humans makes it an attractive target for the development of novel antibiotics and herbicides.[20,21] KPR belongs to the 6-phosphogluconate dehydrogenase superfamily in the SCOP database[22] and has properties of both class A and class B secondary alcohol dehydrogenases.[23] The enzyme has been characterized both biochemically and structurally.[23−25] More recently, the crystal structure of KPR with $NADP^+$ bound at the active site was solved.[26] The cofactor-binding site is a long cleft encompassing the active site between two domains. The nicotinamide ring of the cofactor adopts a *syn* conformation, and stereospecific hydride transfer is from the *pro-S* proton of NADPH to the *si* face of ketopantoate (Scheme 1).[23,26] Although it has been recently reported that the *E. coli* enzyme can use NADH as a cofactor, KPR is an NADPH-specific dehydrogenase.[23,24] NADPH binds to apo-KPR with high affinity (K_d = 300 nM).[26] To elucidate which parts of the NADPH structure contribute most to binding, we have used smaller fragments and analogues of the cofactor as probe ligands (Figure 1). To assess the ability of cofactor fragments to bind to KPR, biophysical studies were conducted using NMR spectroscopy, kinetic inhibition studies, ITC, and site-directed mutagenesis. The aims and motivations of our work were 3-fold: first, to identify potential hot spots at the cofactor-binding site, second, to elucidate the structural determinants of cofactor specificity, and third, to study the effects of growing small molecular fragments on inhibition of the enzyme.

* To whom correspondence should be addressed. Phone: +44-1223-336405. Fax: +44-1223-336362. E-mail: ca26@cam.ac.uk.
[†] University Chemical Laboratory, University of Cambridge.
[‡] Astex Therapeutics Ltd.
[§] Department of Plant Sciences, University of Cambridge.
[||] Department of Biochemistry, University of Cambridge.

10.1021/jm060490r CCC: $33.50
Published on Web 07/08/2006

Scheme 1. Reaction Catalyzed by Ketopantoate Reductase

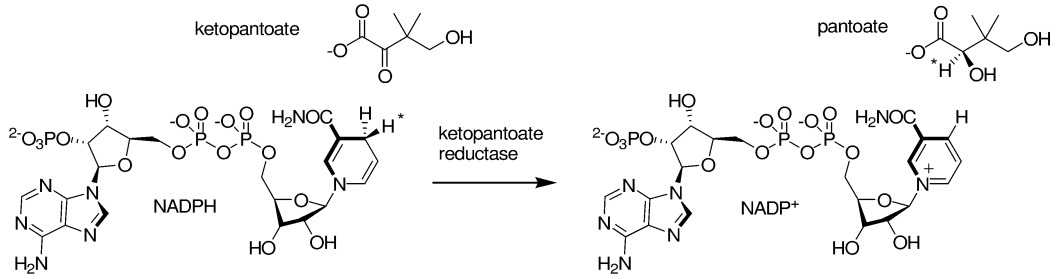

Results

Selection of Cofactor Analogues. We applied a fragment-based approach that involves the breaking down of NADPH, the large cofactor in the reaction catalyzed by KPR (MW = 740, K_d = 300 nM), into smaller fragments and analogues, to probe for interactions at the cofactor-binding site. The compounds studied (Figure 1) included (i) dinucleotides lacking the 2′-phosphate−NAD^+ and NADH, (ii) pyridine fragments−β-NMN and nicotinamide, (iii) adenosyl fragments lacking the 2′-phosphate−AMP, ADP, and ADP-ribose, (iv) adenosyl fragments containing the 2′-phosphate−2′P-AMP and 2′P-ADP-ribose, and (v) nucleotide analogues−ATP, GDP, and GTP.

A related approach was earlier described by Stout et al. using X-ray crystallography to study the interaction of the enzyme thymidylate synthase with fragments of its substrate dUMP.[27] X-ray crystallography allows the identification of the precise binding interactions of fragments with the protein;[9,12] however, it does not reveal direct information on ligand affinity. Our approach combined inhibition studies with direct binding studies using NMR spectroscopy and ITC. All these experiments were conducted using His_6-KPR at pH 7.5−7.7, under optimal conditions for enzyme solubility and ligand stability. This protein construct was catalytically active, with kinetic parameters k_{cat} = 25 s^{-1}, $K_{M(NADPH)}$ = 7 μM, and $K_{M(ketopantoate)}$ = 30 μM, comparable to those of the native enzyme.[23,25]

Isothermal Titration Calorimetry. To determine the contributions of individual groups on the cofactor to the binding affinity and enthalpic and entropic components of the free energy of binding, the thermodynamics of the interaction of His_6-KPR with cofactor analogues was characterized using ITC (Table 1). Since the dissociation constants measured for cofactor analogues were relatively weak in all cases (K_d > 50 μM), K_d was generally higher than the protein concentrations used in the experiments; therefore, the c value ($c = [P]_t/K_d$) was lower than 1. Under low c value conditions, both ΔG and ΔH can be measured with confidence provided at least 80% saturation of the enzyme is achieved at the end of the titration and the stoichiometry n is known, as described by Turnbull and Danaras.[28] The stoichiometry (n = 1) was determined independently by performing active site titration experiments with NADPH or $NADP^+$ under high c values (see the Experimental Section).

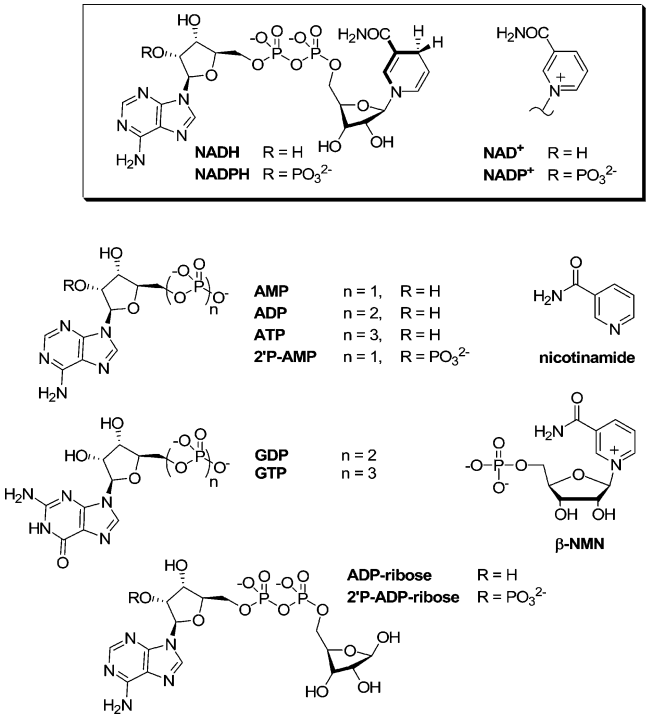

Figure 1. Chemical structures of NADPH analogues used in this study.

Table 1. Thermodynamic Parameters of Nucleotides Binding to *E. coli* KPR[a]

ligand	no. of expts	K_d (μM)	ΔG (kcal/mol)	ΔH (kcal/mol)	$-T\Delta S$ (kcal/ mol)
NADPH	2	0.26 ± 0.11	−9.08 ± 0.27	−3.09 ± 0.10	−6.00 ± 0.38
$NADP^+$	3	5.8 ± 0.8	−7.21 ± 0.08	−3.16 ± 0.06	−4.05 ± 0.11
AMP	1	>5000	nd	nd	nd
ADP	3	360 ± 15	−4.73 ± 0.03	−2.6 ± 0.3	−2.1 ± 0.3
ATP	3	130 ± 20	−5.35 ± 0.09	−3.1 ± 0.1	−2.3 ± 0.1
ADP-ribose	1	6300 ± 500	−3.02 ± 0.04	nd	nd
β-NMN	1				
nicotinamide	1				
NADH	2	66 ± 6	−5.75 ± 0.06	−2.9 ± 1.3	−2.8 ± 1.3
NAD^+	1	6900 ± 300	−2.97 ± 0.03	−5.9 ± 0.2	2.9 ± 0.2
GDP	1	373 ± 13	−4.70 ± 0.01	−3.6 ± 0.1	−1.1 ± 0.1
GTP	2	153 ± 12	−5.25 ± 0.05	−5.8 ± 0.1	0.6 ± 0.1
2P′-AMP	2	100 ± 15	−5.49 ± 0.09	−3.1 ± 0.1	−2.4 ± 0.1
2P′-ADP-ribose	2	61 ± 8	−5.80 ± 0.07	−3.0 ± 0.3	−2.8 ± 0.4

[a] ITC titrations were performed in 0.1 M HEPES/HCl, pH 7.7, at 27 °C. Errors quoted are those returned by Origin on the curve fitting (no. of expts = 1) or standard deviations of multiple experiments (no. of expts > 1). The stoichiometry for weak-affinity ligands (K_d > 100 μM) was fixed at n = 1, the value being determined from active site titration experiments with NADPH or $NADP^+$. nd = not determined.

The smallest fragment for which binding could be detected was AMP. However, the binding affinity was very weak (K_d > 5 mM), and a low heat signal prevented an accurate determination of the thermodynamic parameters. In contrast, binding of ADP and ATP was fully characterized by ITC. Dissociation constants of 360 and 130 μM and enthalpies of binding of −2.6 and −3.1 kcal/mol were obtained for ADP and ATP, respectively. To investigate the requirement for the adenosyl moiety further, GDP and GTP were also tested. Dissociation constants of 370 and 150 μM were obtained, comparable with those for ADP and ATP, respectively. NAD^+ and ADP-ribose were found to bind weakly, with estimated dissociation constants of 7 and 6.3 mM, respectively. No binding was observed for nicotinamide and β-NMN, in agreement with NMR and inhibition results (see also Tables 2 and 3). NADH showed the highest affinity among the analogues lacking the 2′-phosphate, with a K_d of 70 μM. Fragments containing the 2′-phosphate group showed relatively

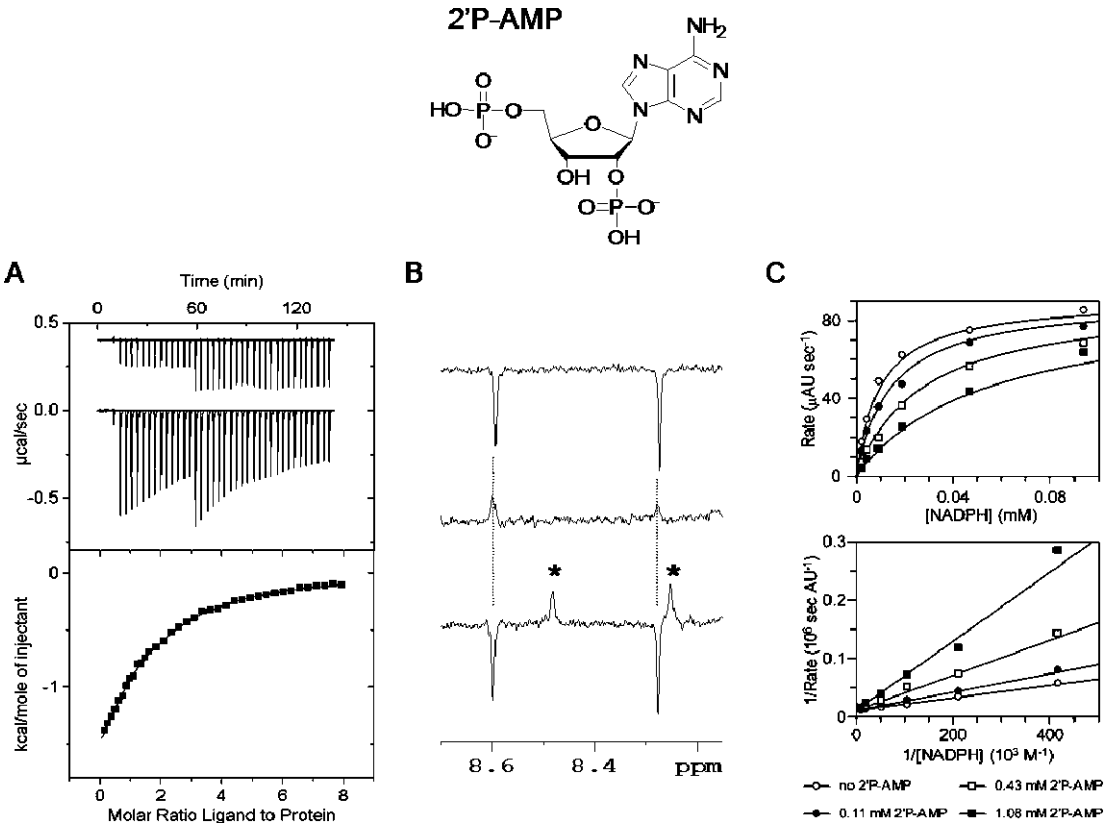

Figure 2. Binding and inhibition studies of KPR with 2′P-AMP. (A) ITC analysis at 27 °C. Top panel: Raw data for titrations of 2.4 mM ligand into 60 μM protein (lower trace) and buffer (upper trace). Each peak corresponds to one injection. An initial 1 μL injection was followed by 13 × 4 and 24 × 8 μL injections. Bottom panel: Integration of the data, corrected for the heat of dilution. The line represents the least-squares fit to the single-site binding model by the ORIGIN program. (B) WaterLOGSY binding experiment. From top to bottom, NMR spectra of 0.5 mM 2′P-AMP recorded (i) in the absence of KPR, (ii) in the presence of 20 μM KPR, and (iii) the same as above, with NADPH added to a final concentration of 350 μM. LOGSY signals for NADPH are highlighted by asterisks. (C) Steady-state inhibition analysis versus NADPH. Data were fitted to the equation for competitive inhibition, and a K_i of 240 ± 20 μM was obtained.

strong affinity by ITC. A typical titration is shown in Figure 2A for 2′P-AMP. Dissociation constants of 100 and 60 μM and ΔH values of binding of −3.1 and −3.0 kcal/mol were obtained for 2′P-AMP and 2′P-ADP-ribose, respectively (Table 1).

Binding Specificity. We have recently used WaterLOGSY ^{1}H NMR binding experiments to detect binding of cofactors and substrates to His$_6$-KPR.[11,26] WaterLOGSY is a rapid 1D ^{1}H NMR spectroscopic technique to detect binding of small molecules to a target protein in solution.[29,30] In WaterLOGSY, the signals are generated by cross-relaxation from bulk water. Due to the very different tumbling times of the free ligand and of the protein−ligand complex, LOGSY signals are typically negative for free ligands in solution, and relatively less negative or positive for binders in the presence of the protein.[11,29]

Cofactor analogues were initially screened at 1 mM concentration by WaterLOGSY, and NADPH was subsequently added to displace the bound ligands and to show specific interactions at the cofactor-binding site (Table 2). The adenine mononucleotides AMP, ADP, and ATP were found to bind to KPR by WaterLOGSY. The ligands were successfully displaced by the addition of NADPH to a final concentration of 350 μM, thereby proving specific binding at the active site.[11] In contrast, binding of nicotinamide, β-NMN, ADP-ribose, or NAD$^+$ was not detected under identical conditions, their LOGSY spectra showing no significant changes in the presence of the protein. In contrast, fragments 2′P-AMP and 2′P-ADP-ribose generated relatively large LOGSY effects at 0.5 mM concentration (Table 2). A competition WaterLOGSY NMR experiment between 2′P-AMP and NADPH is shown in Figure 2B.

Table 2. Screening of KPR with Cofactor Analogues by WaterLOGSY NMR Spectroscopy[a]

ligand	singlet NMR signal obsd (ppm)	LOGSY effect[b] (%)	displacement by NADPH
NADPH	8.47	200	
NADP$^+$	9.30	210	nd
AMP	8.27	30	yes
ADP	8.27	90	yes
ATP	8.27	130	yes
ADP-ribose	8.27	0	nd
β-NMN	9.59	0	nd
nicotinamide	8.94	0	nd
NAD$^+$	9.34	10	yes
2P′-AMP[c]	8.28	115	yes
2P′-ADP-ribose[c]	8.29	160	yes

[a] Ligand and protein concentrations were 1 mM and 50 μM, respectively. NADPH was added to a final concentration of 0.35 mM to displace ligands bound in the cofactor-binding site. nd = not determined. [b] LOGSY effects are the relative percent differences, $[(I_p - I_f) \times 100]/I_f$, between the intensities of an NMR signal of the ligand in the absence (I_f) and presence (I_p) of the protein. In the absence of binding the two intensities are equal, resulting in a null effect (0%). When binding occurs, I_p is smaller than I_f, so the LOGSY effect is positive. [c] Ligand and protein concentrations were 0.5 mM and 20 μM, respectively.

The binding specificity of adenine nucleotides was further demonstrated using competitive ITC experiments. This indirect approach allows studying the weak interaction of the fragment of interest by displacement with a known high-affinity ligand. Titrations of His$_6$-KPR with NADPH were performed in the absence and in the presence of the fragment under otherwise identical conditions.[11] The K_d and ΔH for NADPH obtained from the two titrations were used to estimate the K_d and ΔH

Table 3. Inhibition of *E. coli* KPR by Analogues of NADPH

ligand	response[a]	K_i[b] (mM)	inhibition[c]
phosphate		27 ± 4	C
AMP		6.3 ± 0.9	C
ADP		1.05 ± 0.07	C
ATP		0.61 ± 0.04	NC
ADP-ribose	0% at 5 mM		
β-NMN	0% at 5 mM		
nicotinamide	0% at 11 mM		
NADH		K_M = 0.75 mM	
NAD^+	10% at 20 mM		
2′-AMP		0.24 ± 0.02	C
2′-ADP-ribose		0.20 ± 0.02	C

[a] Ligands were initially tested for inhibition at 1 mM concentration with 20 μM NADPH, 1 mM ketopantoate, and 2 nM KPR. Response is not shown for the inhibitors with measured K_i. [b] Inhibition analysis was accomplished with five different inhibitor concentrations and six concentrations of NADPH. [c] The varied substrate was NADPH. C = competitive, and NC = noncompetitive.

for the weak competitor ligand, by applying the displacement model described by Zhang and Zhang[31] and Sigurskjold.[32] The resulting binding parameters of fragments were found to be in good agreement with those obtained by direct ITC titrations at a low *c* value.[11]

Kinetic and Inhibition Studies. To validate the ITC and NMR results and to confirm the ligands identified are inhibitors, compounds were initially tested at 1 mM concentration for activity against His_6-KPR. Adenine nucleotides AMP, ADP, ATP, 2′P-AMP, and 2′P-ADP-ribose were found to inhibit KPR activity (Table 3). In contrast, no significant inhibition was observed for nicotinamide, β-NMN, and ADP-ribose, even when tested at higher concentrations (Table 3). NAD^+ showed only 10% inhibition when tested at 20 mM. All these results were consistent with those from both ITC and NMR binding studies (see above).

Full binding curves for the active adenine analogues were then measured using five different inhibitor concentrations and six concentrations of NADPH. ADP and ATP had K_i values of 1 and 0.6 mM, respectively, and AMP was by far the weakest in the series (K_i = 6 mM). Interestingly, while AMP and ADP showed competitive inhibition against NADPH, ATP inhibition was noncompetitive (data not shown). 2′P-AMP and 2′P-ADP-ribose were the most potent among the inhibitors tested. Both inhibitors were competitive against NADPH, with K_i values of 240 and 200 μM, respectively (see Figure 2C for 2′P-AMP).

Design of Mutants To Probe the Binding Site. To provide structural information on the interaction of fragments, in addition to that given by competitive binding studies, site-specific mutants were designed to locate the ligand-binding sites. The crystal structure of the KPR/$NADP^+$ binary complex[26] was inspected to provide details of the interactions between the cofactor and residues at the active site (Figure 3). Arg31 and Asn98 were chosen as they are located at the two opposite ends of the cofactor-binding site (Figure 3). Arg31 is involved in strong electrostatic and hydrogen-bonding interactions with the adenosyl 2′-phospate group of $NADP^+$. Amino acid sequence alignments with other bacterial KPRs identify Arg31 of the *E. coli* enzyme as a conserved residue. In KPR primary sequences it occurs about 20 residues downstream of the last glycine in the conserved GXGXXG motif for dinucleotide recognition. Other NADP(H)-specific dehydrogenases have an arginine residue binding the 2′-phosphate in an analogous position.[33−35] Consequently, the R31A mutant was used to monitor interactions in the adenosyl-binding pocket. Similarly, Asn98 was mutated to Ala to monitor interactions in the nicotinamide pocket of the cofactor-binding site. Asn98 is another strictly conserved

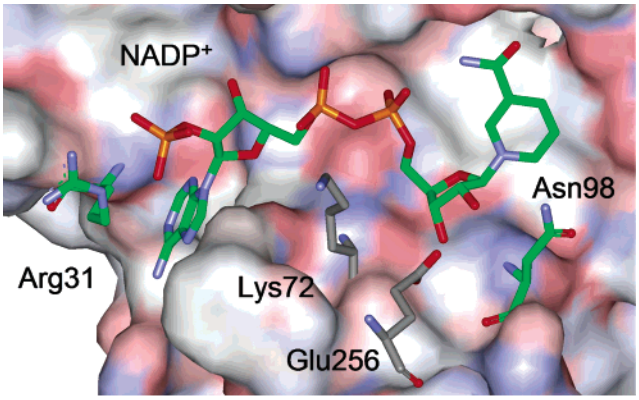


```
          7 9 12          31                              98
ECOLI   ~~VLGCGALGQL~~~GWLRVPQ~~~~~~~~~~~~~~LLIHNGMGT~~~
AQUAE   ~~IVGVGAIGSA~~~GLVRRNP~~~~~~~~~~~~~~MIAQNGYGN~~~
ARCFU   ~~IMGAGALGSL~~~FVARGKQ~~~~~~~~~~~~~~CSLQNGVGN~~~
BACSU   ~~IIGGGSVGLL~~~VTRRQEQ~~~~~~~~~~~~~~LFLQNGMGH~~~
PSEAE   ~~ILGAGSLGSL~~~LILRDRQ~~~~~~~~~~~~~~LLLQNGLGS~~~
PYRAB   ~~ILGAGAIGSL~~~LIGRDPH~~~~~~~~~~~~~~LSIQNGIGN~~~
PYRHO   ~~ILGAGAIGSL~~~LIGRGRH~~~~~~~~~~~~~~LSLQNGIGN~~~
SALTY   ~~VLGCGALGQL~~~GWLRVPQ~~~~~~~~~~~~~~LLIHNGMGT~~~
VIBCH   ~~VLGPGAVGSL~~~LWSRQAQ~~~~~~~~~~~~~~LFMHNGMGA~~~
YERPE   ~~VLGCGALGQL~~~GWLRVPQ~~~~~~~~~~~~~~LLLHNGMGT~~~
          * *  *       *                               *
```

Figure 3. Selection of mutants to probe fragment binding. Binding mode of $NADP^+$ (green carbons) observed in the crystal structure of the binary complex.[26] The enzyme active site (residues 1−170) is shown as a solvent-accessible surface, colored by atom charges (neutral, white; positive, blue; negative, red). Arg31 and Asn98 (green carbons) interact with the cofactor at opposite ends of the active site. ClustalW sequence alignment of 10 bacterial ketopantoate reductases highlights the conservation of both residues. The organism accession codes are as follows: *Escherichia coli* (ECOLI); *Aquifex aeolicus* (AQUAE); *Archaeoglobus fulgidus* (ARCFU); *Bacillus subtilis* (BACSU); *Pseudomonas aeruginosa* (PSEAE); *Pyrococcus abyssi* (PYRAB); *Pyrococcus horikoshii* (PYRHO); *Salmonella typhimurium* (SALTY); *Vibrio cholerae* (VIBCH); *Yersinia pestis* (YERPE).

residue among bacterial KPRs (Figure 3). It forms hydrogen bonds to the nicotinamide ribose 2′- and 3′-hydroxyls of $NADP^+$ and has been recently identified as important for enzyme catalysis and substrate binding.[26] It was assumed that neither of these mutations would lead to significant structural changes in the active site.

Calorimetric Analysis of the Effect of R31A and N98A Mutations. Combining ITC with site-directed mutagenesis provides a sensitive thermodynamic probe to identify the effects of specific residues in interactions with ligands. This approach was employed to locate the binding site of cofactor fragments. Titrations of KPR R31A and N98A mutants with adenine nucleotides—2′P-ADP-ribose, 2′P-AMP, ADP, and ATP—were conducted using ITC under the same conditions used for the wild-type (WT) enzyme. Similar experiments were also conducted with $NADP^+$ as a reference. Thermodynamic data for KPR mutants are compared to those for WT KPR in Table 4. Results are reported as $\Delta\Delta G$ [$\Delta G_{mutant} - \Delta G_{WT}$] together with the relative contributions from $\Delta\Delta H$ [$\Delta H_{mutant} - \Delta H_{WT}$] and $-T\Delta\Delta S$ [$-T(\Delta S_{mutant} - \Delta S_{WT})$].

The point mutation of Arg31 to Ala decreases the affinity of all adenine nucleotides (Table 4), suggesting Arg31 is involved in binding the ligands. The largest effects upon the R31A mutation were $\Delta\Delta G$ values of 2.5 and 2.1 kcal/mol for 2′P-AMP and 2′P-ADP-ribose, respectively, corresponding to 60- and 30-fold decreases in affinity. These results are consistent with that observed for $NADP^+$, where the R31A mutation resulted in a $\Delta\Delta G$ of 1.6 kcal/mol. The weak affinities of the

Table 4. Effect of Point Mutations on the Thermodynamic Parameters of Nucleotide Binding[a]

	R31A			N98A		
ligand	$\Delta\Delta G$ (kcal/mol)	$\Delta\Delta H$ (kcal/mol)	$-T\Delta\Delta S$ (kcal/mol)	$\Delta\Delta G$ (kcal/mol)	$\Delta\Delta H$ (kcal/mol)	$-T\Delta\Delta S$ (kcal/mol)
$NADP^+$	1.6	0.9	0.7	−1.5	−2.0	0.5
2P′-ADP-ribose	2.1	nd	nd	−0.6	−2.3	1.7
2P′-AMP	2.5	nd	nd	0.1	0.1	<0.1
ADP	0.8	0.5	0.3	−0.1	−0.1	<0.1
ATP	0.5	1.7	−1.2	<0.1	−1.2	1.2

[a] $\Delta\Delta G$, $\Delta\Delta H$, and $-T\Delta\Delta S$ are $\Delta G_{mutant} - \Delta G_{WT}$, $\Delta H_{mutant} - \Delta H_{WT}$, and $-T(\Delta S_{mutant} - \Delta S_{WT})$, respectively. ITC titrations were performed in 0.1 M HEPES/HCl, pH 7.7, at 27 °C. nd = not determined.

2′-phosphate-containing fragments with the R31A mutant prevented accurate determinations of the binding ΔH and ΔS. The $\Delta\Delta G$ values for ADP and ATP binding with R31A relative to WT KPR were 0.8 and 0.5 kcal/mol, respectively. However, the relative enthalpic and entropic contributions were different, with $\Delta\Delta H$ and $-T\Delta\Delta S$ both being positive in the case of ADP and being of opposite sign in the case of ATP (Table 4).

Binding of 2′P-ADP-ribose to the N98A mutant showed a small increase in binding affinity ($\Delta\Delta G = -0.6$ kcal/mol) comprising a negative $\Delta\Delta H$ and a positive $-T\Delta\Delta S$ relative to that to the WT. The signatures of the thermodynamic binding parameters with N98A are in agreement with those observed for $NADP^+$ and are consistent with interaction of the terminal ribose of 2′P-ADP-ribose with the side chain of Asn98 and with the inclusion of water molecules in the cavity created by the mutation. In contrast, the N98A mutation had no measurable effects on the binding thermodynamics of 2′P-AMP and ADP (Table 4), consistent with Asn98 not interacting with these ligands. This mutation of Asn98 resulted in changes in ΔH and $T\Delta S$ of 1.2 kcal/mol for binding of ATP. However, these changes were compensatory and resulted in no detectable change in ΔG.

Discussion

Structure−activity relationships (SARs) of the compounds in Figure 1 provide insights into the roles of different structural moieties on cofactor recognition and specificity and into the effects of growing fragments on the binding affinity. Within a chemical series it is often observed that affinity is strongly correlated with molecular weight.[36−38] Through an analysis of the energetics of protein−ligand complexes, Kuntz et al. noted that the affinity of a ligand for its target protein increases linearly with respect to the number of non-hydrogen atoms (NHA) for very small compounds (NHA < 10−15).[36] However, this linear tendency is broken for larger compounds as adding more atoms no longer corresponds to an increase in the binding energy. Therefore, the resulting ligand efficiency ($\Delta g = \Delta G/(\text{NHA})$) tends to be maximal for small molecular fragments and then steadily decreases as more heavy atoms are added. Ligand efficiency allows a reliable assessment of different chemical scaffolds and is often useful in deciding the potential for optimization of hit compounds.[37,38]

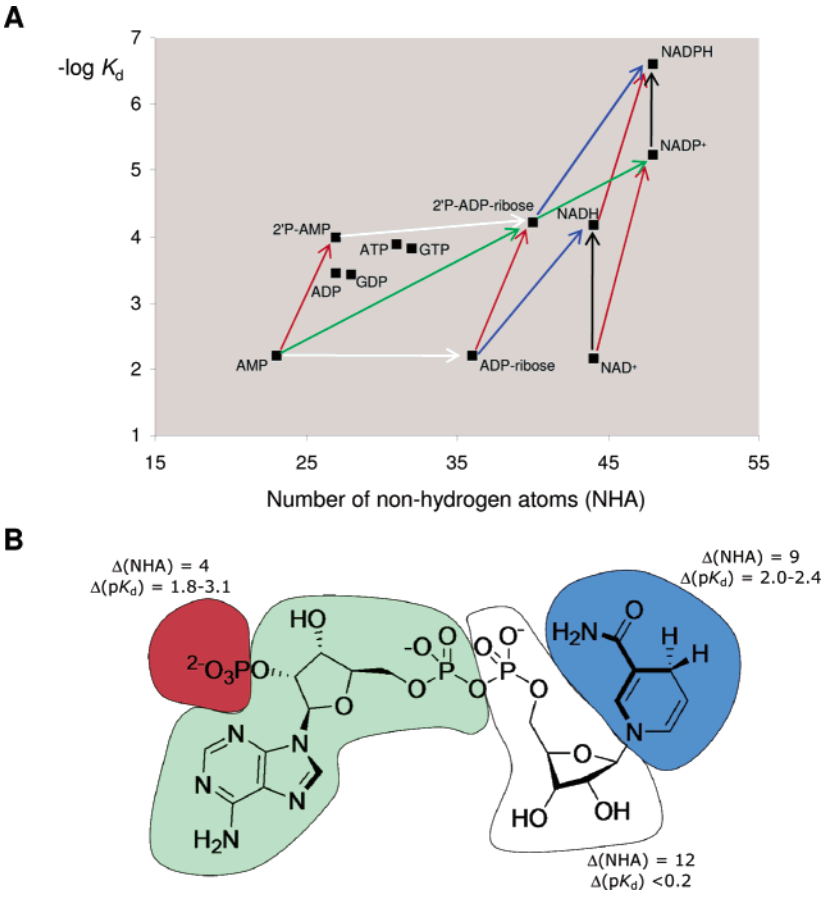

Figure 4. Ligand efficiency of cofactor analogues and fragments. (A) Affinity (logarithmic scale) versus number of non-hydrogen atoms. Growing AMP → 2′P-ADP-ribose → $NADP^+$ (green arrows) maintains ligand efficiency approximately constant. Addition of the 2′-phosphate group (red arrows), the 1,4-dihydronicotinamide ring (blue arrows), and a hydride ion to the oxidized nicotinamide ring (black arrows) increases ligand efficiency. In contrast, addition of the β-phosphate−ribose fragment (white arrows) decreases ligand efficiency. (B) Fragmentation of NADPH and relative contributions to affinity. The starting fragment AMP is circled in green. The ligand-efficient 2′-phosphate and reduced nicotinamide groups are circled in red and blue, respectively. The ligand-inefficient β-phosphate−ribose fragment is circled in white.

Trends in Ligand Efficiency of Cofactor Fragments. Here we use the concept of ligand efficiency to identify unambiguously the structural determinants for the binding affinities. To illustrate the trend of ligand efficiency within our chemical series, a plot of affinity (logarithmic scale) versus NHA is shown in Figure 4A. The average Δg of cofactor analogues was 0.15 $\pm$ 0.04 kcal·mol^{-1}·NHA^{-1}, which is smaller than the generally accepted lower limit for Δg of drug leads of around 0.3 kcal·mol^{-1}·NHA^{-1}.[37,38] This suggests that the ligands studied would not be good starting points for fragment-based drug design. However, analysis of this series of cofactor fragments based on their ligand efficiency provides important insights into potential hot spots at the cofactor-binding site for future design of inhibitors.

AMP, albeit one of the weakest binders in the series, is also the smallest fragment for which binding or inhibition could be detected (Tables 2 and 3). The ligand efficiency of AMP ($\Delta g = 0.13$) is comparable to the average in the series, making it a good starting point in the discussion of the effect of growing fragments (green fragment, Figure 4B). Growing AMP → 2′P-ADP-ribose → NADP$^+$ maintains the ligand efficiency approximately constant (green arrows in Figure 4A). Growing fragments with improvements of ligand efficiency will lead to arrows having higher slopes than the green arrows (e.g., red, blue and black arrows in Figure 4A). In contrast, growing fragments with decreases in ligand efficiency will correspond to arrows with lower slopes (e.g., white arrows).

Addition of the 2′-phosphate group (Δ(NHA) = 4) to AMP leads to the most efficient fragment 2′P-AMP ($\Delta g = 0.20$). Similarly, addition of the 2′-phosphate group to other fragments always leads to large increases in affinity ($\Delta pK_d = 1.8-3.1$) and consequently to increases in ligand efficiency (red arrows). The 2′-phosphate is thus a ligand-efficient group (red moiety in Figure 4B, left). Addition of the 1,4-dihydronicotinamide ring (Δ(NHA) = 9) also leads to significant increases in potency ($\Delta pK_d = 2.0-2.4$). The reduced nicotinamide is a second ligand-efficient group (blue moiety in Figure 4B, right), albeit to a smaller extent than the 2′-phosphate group as shown by comparing the blue and red arrows in Figure 4A. Therefore, the corresponding binding sites on the protein are hot spots. Interestingly, the most ligand-efficient structural modification is the addition of a single hydride ion to the oxidized nicotinamide ring to form the 1,4-dihydronicotinamide ring (black arrows in Figure 4A).

In contrast, addition of the large β-phosphate−ribose fragment (Δ(NHA) = 12) does not significantly improve the affinity (white arrows in Figure 4A). This part of the cofactor is therefore ligand-inefficient (white fragment in Figure 4B). These observations are consistent with the β-phosphate−ribose moiety acting as a linker between the binding-anchor adenosyl group and the chemically reactive nicotinamide ring and providing the correct conformation for catalysis. Addition of the oxidized nicotinamide group also does not increase the ligand efficiency. Furthermore, small fragments containing the oxidized pyridine ring (β-NMN and nicotinamide) did not bind to KPR at 5−10 mM concentration. As a result, the least efficient ligand with detectable affinity was NAD$^+$ ($\Delta g = 0.07$), which is formed by addition of the scaffolds β-phosphate−ribose and oxidized nicotinamide to AMP.

Effects of 2′-Phosphate and Nicotinamide Groups. Although KPR is an NADPH-specific dehydrogenase, activity of the *E. coli* enzyme was recently reported using NADH as a cofactor.[24] We tested NADH as a cofactor and obtained a K_M of 750 μM (Table 3) and a k_{cat} of 95 s^{-1}, resulting in an approximately 25-fold decrease of k_{cat}/K_M relative to that of NADPH. *E. coli* KPR was also previously shown to bind NADPH more tightly than NADP$^+$.[26] This selectivity may be important in encouraging cofactor dissociation after hydride transfer (Scheme 1).

The biophysical studies presented here provide additional quantitative evidence that KPR binds selectively to 2′-phosphate nucleotides in preference to the corresponding 2′-hydroxyl nucleotides and to the reduced nicotinamide in preference to the oxidized nicotinamide group. The increases in binding affinities observed by ITC for the addition of the 2′-phosphate group were 100−1200-fold, and those for replacing the oxidized with the reduced nicotinamide group were 20−100-fold (Table 1). In the latter case, the more favorable ΔG arises almost entirely from a more favorable binding entropy, with $T\Delta\Delta S$ values of 2 and 6 kcal/mol for NADPH versus NADP$^+$ and NADH versus NAD$^+$, respectively (Table 1). These observations suggest that the nicotinamide-binding site is predominantly apolar in nature, strongly favoring binding of hydrophobic compounds. Consistent with this hypothesis, inspection of the KPR/NADP$^+$ structure shows that the nicotinamide group sits in a predominantly hydrophobic pocket (Figure 3). The identification of the 2′-phosphate and reduced nicotinamide as key groups for cofactor recognition is consistent with the presence of two distinct hot spots at the cofactor-binding site.

Binding Modes of Fragments and Adenine Recognition. The addition of the same group to different fragments of NADPH was found to produce similar increases in affinity, as can be seen in Figure 4A where arrows of the same color are parallel. This observation strongly suggests a conservation of binding modes across the series of fragments, presumably consistent with the binding mode observed for NADP$^+$ (Figure 3).[26] To provide additional structural evidence on fragment binding, Arg31 and Asn98 were mutated to Ala to monitor interactions at hot spots on opposite ends of the cofactor-binding site (Figure 3). Small changes in intermolecular interactions often lead to enthalpy−entropy compensation, thereby masking changes in the binding free energy.[39−41] The advantage of using ITC is that the effects of a mutation on the binding ΔH and ΔS are also characterized.

The ITC results with alanine mutants show that Arg31 is strongly involved in the binding of 2′P-AMP and 2′P-ADP-ribose (Table 4), suggesting these fragments adopt the same binding mode as NADP$^+$. The results with N98A KPR support this conclusion. The decreases in binding affinity of these fragments upon replacing Arg31 to Ala (30−60-fold) are in good agreement with those arising from deleting the 2′-phosphate group (60−100-fold). These observations support the proposal of a key interaction between the 2′-phosphate group and the side chain of Arg31 and further reinforce our approach to accurately define the SAR for weakly binding fragments.

ADP and ATP also appear to interact with Arg31 at the adenosyl-binding pocket, despite the lack of the key 2′-phosphate group. The affinity trend AMP $\ll$ ADP < ATP is seen in both the inhibition and calorimetric data, and supported by WaterLOGSY studies (Tables 1−3). The stepwise addition of a phosphate group at the 5′ position of the adenosyl ribose group is therefore thermodynamically favored. In contrast to ADP and NADP$^+$, ATP binding shows significant $\Delta H - \Delta S$ compensation upon mutation of both Arg31 and Asn98, suggesting that the presence of a γ-phosphate group may facilitate small structural rearrangements on ligand binding, leading to additional contributions to ΔH and $T\Delta S$. The observed noncompetitive inhibition of ATP versus NADPH may arise from

multiple binding modes or binding to a different form of the enzyme, rather than from simultaneous binding with NADPH. This interpretation is further supported by the unusual binding thermodynamics displayed by ATP with the mutant proteins.

Interestingly, the adenosyl group was found not to be a stringent requirement for binding, as demonstrated by the relatively strong affinities of GDP and GTP (Table 1). Such promiscuous binding is consistent with the theory of fuzzy recognition of the adenosyl group proposed by Thornton and co-workers.[42] An inspection of the crystal structure of the KPR/$NADP^+$ complex shows that the adenine-binding pocket is rather solvent-exposed and can potentially accommodate the adenine−guanine substitution.

Conclusions

Targeting families of enzymes such as dehydrogenases and kinases at the cofactor-binding site is an important drug design strategy. We have mapped the active site of a model dehydrogenase, ketopantoate reductase, using fragments derived from its cofactor NADPH. Two hot spots were characterized at opposite ends of the binding surface which contribute high affinity and significant increases in ligand efficiency. On the basis of our study, structural requirements for cofactor recognition that define a blueprint for future inhibitor design have been identified. We are now specifically targeting these hot spots at the cofactor-binding site of KPR using fragment-based approaches.

In this paper we report the first application of low *c* value ITC for dissecting the binding contributions of individual fragments of a ligand and extend the arsenal of techniques available for studying low-affinity interactions in fragment-based drug design. The combination of ITC and alanine-scanning mutagenesis as a tool to locate binding of fragments is also described. The major advantage of this approach is that it provides the complete thermodynamic characterization of the effect of mutations to ligand binding. This, in turn, enables not only unambiguous identification of the location of hot spots on protein surfaces but also definition of their structural and energetic properties. The approach described holds general applicability to study other enzymes and may prove useful to fragment-based drug discovery.

Experimental Section

Materials. All chemicals were purchased from Sigma-Aldrich unless otherwise stated. Accurate concentrations of cofactor fragments and analogues were measured by UV/vis spectrophotometry using the following extinction coefficients: 6220 M^{-1} cm^{-1} at 340 nm for NADPH and NADH;[43] 18000 M^{-1} cm^{-1} at 260 nm for $NADP^+$ and NAD^+;[44] 15400 M^{-1} cm^{-1} at 259 nm for AMP, ADP, and ATP;[45] 4200 M^{-1} cm^{-1} at 266 nm for β-NMN;[46] 13700 M^{-1} cm^{-1} at 253 nm for GDP and GTP;[45] 15400 M^{-1} cm^{-1} at 260 nm for 2′P-AMP and 2′P-ADP-ribose.[47,48]

Protein Expression and Purification. Wild-type KPR and site-directed mutants of KPR were expressed from a pRSETA plasmid, which adds 17 amino acid residues to the N-terminus of the recombinant protein, including a His_6 tag. KPR proteins were expressed in *E. coli* and purified using a single-step affinity purification column as previously described.[26] Briefly, C41(DE3) cells containing the pRSETA-*panE* plasmid encoding *E. coli* ketopantoate reductase were grown in 2×YT medium containing 100 μg/mL ampicillin at 37 °C and induced with 0.5 mM IPTG for 4 h. Cells were collected and resuspended in 50 mM potassium phosphate, pH 8.0, 10 mM imidazole, 300 mM NaCl, 0.007% v/v β-mercaptoethanol, 1 mM PMSF, and 0.5%, v/v, protease inhibitor cocktail. Cells were lysed by incubation with 0.2 mg/mL lysozyme for 30 min at room temperature followed by sonication, for a total process time of 3 min. His_6-KPR was applied to a Ni−NTA column (Qiagen), washed with 50 mM potassium phosphate, pH 8.0, 30 mM imidazole, and 300 mM NaCl, and eluted with 250 mM imidazole to yield 50−100 mg of His_6-KPR from a 1 L culture. Fractions containing KPR were buffer-exchanged in 100 mM HEPES/HCl, pH 7.6, using a HiPrep 26/10 desalting column (Amersham Bioscience) and further dialyzed in the desired buffer with Slide-A-Lyzer dialysis cassettes (Pierce). Protein concentration was determined by A_{280}, with an extinction coefficient for His_6-KPR of 62650 $M^{-1}cm^{-1}$ obtained from amino acid analysis (PNAC). Protein identity and purity were confirmed by SDS−PAGE and electrospray mass spectrometry.

Site-Directed Mutagenesis. The singly mutated genes corresponding to R31A and N98A were made with the QuickChange site-directed mutagenesis kit (Stratagene) according to the manufacturer's instructions using pRSETA-*panE* as a template. The following primers (SIGMA Genosys) were used for PCR, CAGGGCTGGCTG*GCC*GTACCGCAACCTTA (R31A forward), TAAGGTTGCGGTAC*GGC*CAGCCAGCCCTG (R31A reverse), CGCCAATACTGTTAATTCAC*GCA*GGCATGGGCA (N98A forward), and TGCCCATGCC*TGC*GTGAATTAACAGTATTGGCG (N98A reverse), which generate the alanine mutation (italic). To confirm the mutations, the genes were sequenced in their entirety and the molecular masses of the mutant enzymes were determined using electrospray mass spectrometry.

NMR Spectroscopy. All NMR spectra were recorded at 298 K on a Bruker DRX 500 MHz spectrometer equipped with a 5 mm triple TXI cryoprobe with *z* gradients. All NMR samples for ligand screening contained 1 mM ligand, 50 μM enzyme, and 10% D_2O in a buffer composed of 20 mM potassium phosphate, pH 7.2, and 80 mM NaCl. Subsequent binding experiments with 2′-phosphate analogues were performed in 20 mM Tris/HCl, pH 7.5, to prevent competition between the ligands and the phosphate buffer ($K_{i(phosphate)}$ = 30 mM). In all cases, control experiments were carried out using samples where the enzyme was omitted. (Trimethylsilyl)-propionic acid-d_4 (TSP; 20 μM) was present in all samples for calibration purposes. Water suppression was achieved by using a 1.6 s presaturation pulse and a WATERGATE (water suppression by gradient-tailored excitation)[49] gradient spin−echo sequence. WaterLOGSY[29] NMR experiments employed a 20 ms selective Gaussian 180° pulse at the water signal frequency and an NOE mixing time of 1 s.

UV-Based Kinetic Analysis. Enzyme activity was assayed at 25 °C by monitoring the decrease in absorbance at 340 nm over time due to the enzyme-catalyzed oxidation of NADPH to $NADP^+$ ($\epsilon_{340\ nm(NADPH)}$ = 6220 M^{-1} cm^{-1}) in a 96-well plate using a Biotek Powerwave XS plate reader equipped with KC4 v3.2 Biotek instrument software. Nucleotides were initially tested for inhibition at 1 mM concentration with 20 μM NADPH, 1 mM ketopantoate, and 2 nM enzyme. A typical reaction for K_i analysis contained 100 mM HEPES/HCl, pH 7.6, 1−4 nM enzyme, 2.5−50 μM NADPH, and the inhibitors in a total volume of 200 μL. The reaction was initiated by addition of 1 mM ketopantoate. Measurements were obtained at least in duplicate. Initial rates were obtained from the data corresponding to the conversion of the first 10% of the substrate. Data were fitted to the appropriate rate equations using the GraFit software (version 5.0.6, Erithacus Software Ltd., http://www.erithacus.com/grafit/).

Isothermal Titration Calorimetry. ITC experiments were performed at 27 °C on an OMEGA isothermal titration calorimeter (Microcal Inc.). Details on the instrumentation and experimental design are described elsewhere.[50] Purified protein was exhaustively dialyzed with 100 mM HEPES/HCl, pH 7.7, and loaded into the sample cell at a final concentration of 30−80 μM. Sufficient ligand was used to obtain at least 80% saturation of the enzyme at the end of the titration, as estimated using the equation described by Turnbull and Daranas.[28] Typically, 35 injections of 7−8 μL were made at 3−4 min intervals from a 300 μL syringe rotating at 300 rpm. Alternatively, the initial 15 injections were of 3−4 μL and the final 30 injections were 7−8 μL, all at 3−4 min intervals. The heat change accompanying the titration was recorded as differential

power by the instrument and determined by integration of the peak obtained. Titrations of ligand to buffer only were performed to allow baseline corrections. The corrected heat change was then fitted using nonlinear least-squares minimization to obtain the dissociation constants, K_d, the enthalpy of binding, ΔH, and the stoichiometry, n.[50] A stoichiometry of 1, determined from titrations with NADP(H), was fixed during curve fitting of data obtained under low c value conditions. At least two experiments were performed for each ligand at different ligand concentrations to exclude the occurrence of any concentration-dependent phenomena.

Abbreviations

HEPES, 4-(2-hydroxyethyl)-1-piperazineethanesulfonic acid; ITC, isothermal titration calorimetry; KPR, ketopantoate reductase; β-NMN, β-nicotinamide mononucleotide; 2′P-ADP-ribose, 2′-monophosphoadenosine 5′-diphosphoribose; 2′P-AMP, adenosine 2′,5′-diphosphate; WaterLOGSY, water ligand observed via gradient spectroscopy; WT, wild-type.

Acknowledgment. This work was supported by the U.K. Biotechnology and Biological Sciences Research Council (BBSRC; Grant 8/B15141). A.C. also gratefully acknowledges Astex Therapeutics Ltd. and the Gates Cambridge Trust for financial support. We thank Andrew Karplus (Oregon State University) for the gift of 2′-monophosphoadenosine 5′-diphosphoribose, Sarah L. Maslen for assistance with mass spectrometry, and Carina Lobley and Kellie Tuck for early discussions.

References

(1) Kortemme, T.; Baker, D. A simple physical model for binding energy hot spots in protein−protein complexes. *Proc. Natl. Acad. Sci. U.S.A.* **2002**, *99*, 14116−14121.
(2) Delano, W. L. Unraveling hot spots in binding interfaces: Progress and challenges. *Curr. Opin. Struct. Biol.* **2002**, *12*, 14−20.
(3) Arkin, M. R. and Wells, J. A. Small-molecule inhibitors of protein−protein interactions: Progressing towards the dream. *Nat. Rev. Drug Discovery* **2004**, *3*, 301−317.
(4) Hajduk, P. J.; Huth, J. R.; Fesik, S. W. Druggability indices for protein targets derived from NMR-based screening data. *J. Med. Chem.* **2005**, *48*, 2518−2525.
(5) Huth, J. R.; Sun, C. H.; Sauer, D. R.; Hajduk, P. J. Utilization of NMR-derived fragment leads in drug design. *Methods Enzymol.* **2005**, 549−571.
(6) Rees, D. C.; Congreve, M. S.; Murray, C. W.; Carr, R. Fragment-based lead discovery. *Nat. Rev. Drug Discovery* **2004**, *3*, 660−672.
(7) Erlanson, D. A.; McDowell, R. S.; O'Brien, T. Fragment-based drug discovery. *J. Med. Chem.* **2004**, *47*, 3463−3482.
(8) Murray, C. W.; Verdonk, M. L. The consequences of translational and rotational entropy lost by small molecules on binding to proteins. *J. Comput.-Aided Mol. Des.* **2002**, *16*, 741−753.
(9) Hartshorn, M. J.; Murray, C. W.; Cleasby, A.; Frederickson, M.; Tickle, I. J.; Jhoti, H. Fragment-based lead discovery using X-ray crystallography. *J. Med. Chem.* **2005**, *48*, 403−413.
(10) Gill, A. L.; Frederickson, M.; Cleasby, A.; Woodhead, S. J.; Carr, M. G.; Woodhead, A. J.; Walker, M. T.; Congreve, M. S.; Devine, L. A.; Tisi, D.; O'Reilly, M.; Seavers, L. C. A.; Davis, D. J.; Curry, J.; Anthony, R.; Padova, A.; Murray, C. W.; Carr, R. A. E.; Jhoti, H. Identification of novel p38 alpha MAP kinase inhibitors using fragment-based lead generation. *J. Med. Chem.* **2005**, *48*, 414−426.
(11) Ciulli, A.; Abell, C. Biophysical tools to monitor enzyme-ligand interactions of enzymes involved in vitamin biosynthesis. *Biochem. Soc. Trans.* **2005**, *33*, 767−771.
(12) Blundell, T. L.; Jhoti, H.; Abell, C. High-throughput crystallography for lead discovery in drug design. *Nat. Rev. Drug Discovery* **2002**, *1*, 45−54.
(13) Boehm, H. J.; Boehringer, M.; Bur, D.; Gmuender, H.; Huber, W.; Klaus, W.; Kostrewa, D.; Kuehne, H.; Luebbers, T.; Meunier-Keller, N.; Mueller, F. Novel inhibitors of DNA gyrase: 3D structure based biased needle screening, hit validation by biophysical methods, and 3D guided optimization. A promising alternative to random screening. *J. Med. Chem.* **2000**, *43*, 2664−2674.
(14) Raimundo, B. C.; Oslob, J. D.; Braisted, A. C.; Hyde, J.; McDowell, R. S.; Randal, M.; Waal, N. D.; Wilkinson, J.; Yu, C. H.; Arkin, M. R. Integrating fragment assembly and biophysical methods in the chemical advancement of small-molecule antagonists of IL-2: An approach for inhibiting protein−protein interactions. *J. Med. Chem.* **2004**, *47*, 3111−3130.
(15) McGovern, S. L.; Helfand, B. T.; Feng, B.; Shoichet, B. K. A specific mechanism of nonspecific inhibition. *J. Med. Chem.* **2003**, *46*, 4265−4272.
(16) Frenkel, Y. V.; Clark, A. D.; Das, K.; Wang, Y. H.; Lewi, P. J.; Janssen, P. A. J.; Arnold, E. Concentration and pH dependent aggregation of hydrophobic drug molecules and relevance to oral bioavailability. *J. Med. Chem.* **2005**, *48*, 1974−1983.
(17) Carr, R.; Jhoti, H. Structure-based screening of low-affinity compounds. *Drug Discovery Today* **2002**, *7*, 522−527.
(18) Lundqvist, T. The devil is still in the details − Driving early drug discovery forward with biophysical experimental methods. *Curr. Opin. Drug Discovery Dev.* **2005**, *8*, 513−519.
(19) Webb, M. E.; Smith, A. G.; Abell, C. Biosynthesis of pantothenate. *Nat. Prod. Rep.* **2004**, *21*, 695−721.
(20) Tahiliani, A. G.; Beinlich, C. J. Pantothenic acid in health and disease. *Vitam. Horm.* **1991**, *46*, 165−228.
(21) Begley, T. P.; Kinsland, C.; Strauss, E. The biosynthesis of coenzyme A in bacteria. *Vitam. Horm.* **2001**, *61*, 157−171.
(22) Murzin, A. G.; Brenner, S. E.; Hubbard, T.; Chothia, C. Scop − A structural classification of proteins database for the investigation of sequences and structures. *J. Mol. Biol.* **1995**, *247*, 536−540.
(23) Zheng, R.; Blanchard, J. S. Kinetic and mechanistic analysis of the *E. coli panE*-encoded ketopantoate reductase. *Biochemistry* **2000**, *39*, 3708−3717.
(24) Zheng, R.; Blanchard, J. S. Substrate specificity and kinetic isotope effect analysis of the *Escherichia coli* ketopantoate reductase. *Biochemistry* **2003**, *42*, 11289−11296.
(25) Matak-Vinkovic, D.; Vinkovic, M.; Saldanha, S. A.; Ashurst, J. L.; von Delft, F.; Inoue, T.; Miguel, R. N.; Smith, A. G.; Blundell, T. L.; Abell, C. Crystal structure of *Escherichia coli* ketopantoate reductase at 1.7 Å resolution and insight into the enzyme mechanism. *Biochemistry* **2001**, *40*, 14493−14500.
(26) Lobley, C. M.; Ciulli, A.; Whitney, H. M.; Williams, G.; Smith, A. G.; Abell, C.; Blundell, T. L. The crystal structure of *Escherichia coli* ketopantoate reductase with $NADP^+$ bound. *Biochemistry* **2005**, *44*, 8930−8939.
(27) Stout, T. J.; Sage, C. R.; Stroud, R. M. The additivity of substrate fragments in enzyme-ligand binding. *Structure* **1998**, *6*, 839−848.
(28) Turnbull, W. B.; Daranas, A. H. On the value of *c*: Can low affinity systems be studied by isothermal titration calorimetry? *J. Am. Chem. Soc.* **2003**, *125*, 14859−14866.
(29) Dalvit, C.; Pevarello, P.; Tato, M.; Veronesi, M.; Vulpetti, A.; Sundstrom, M. Identification of compounds with binding affinity to proteins via magnetization transfer from bulk water. *J. Biomol. NMR* **2000**, *18*, 65−68.
(30) Stockman, B. J.; Dalvit, C. NMR screening techniques in drug discovery and drug design. *Prog. Nucl. Magn. Reson. Spectrosc.* **2002**, *41*, 187−231.
(31) Zhang, Y. L.; Zhang, Z. Y. Low-affinity binding determined by titration calorimetry using a high-affinity coupling ligand: A thermodynamic study of ligand binding to protein tyrosine phosphatase 1B. *Anal. Biochem.* **1998**, *261*, 139−148.
(32) Sigurskjold, B. W. Exact analysis of competition ligand binding by displacement isothermal titration calorimetry. *Anal. Biochem.* **2000**, *277*, 260−266.
(33) Lesk, A. M. NAD-binding domains of dehydrogenases. *Curr. Opin. Struct. Biol.* **1995**, *5*, 775−783.
(34) Duax, W. L.; Pletnev, V.; Addlagatta, A.; Bruenn, J.; Weeks, C. M. Rational proteomics I. Fingerprint identification and cofactor specificity in the short-chain oxidoreductase (SCOR) enzyme family. *Proteins: Struct., Funct., Genet.* **2003**, *53*, 931−943.
(35) Wierenga, R. K.; Terpstra, P.; Hol, W. G. Prediction of the occurrence of the ADP-binding beta alpha beta-fold in proteins, using an amino acid sequence fingerprint. *J. Mol. Biol.* **1986**, *187*, 101−107.
(36) Kuntz, I. D.; Chen, K.; Sharp, K. A.; Kollman, P. A. The maximal affinity of ligands. *Proc. Natl. Acad. Sci. U.S.A.* **1999**, *96*, 9997−10002.
(37) Hopkins, A. L.; Groom, C. R.; Alex, A. Ligand efficiency: A useful metric for lead selection. *Drug Discovery Today* **2004**, *9*, 430−431.
(38) Carr, R.; Congreve, M. S.; Murray, C. W.; Rees, D. C. Fragment-based lead discovery: Leads by design. *Drug Discovery Today* **2005**, *10*, 987−992.
(39) Ward, W. H.; Holdgate, G. A. Isothermal titration calorimetry in drug discovery. *Prog. Med. Chem.* **2001**, *38*, 309−376.
(40) Dunitz, J. D. Win some, lose some—Enthalpy−entropy compensation in weak intermolecular interactions. *Chem. Biol.* **1995**, *2*, 709−712.
(41) Holdgate, G. A. and Ward, W. H. Measurements of binding thermodynamics in drug discovery. *Drug Discovery Today* **2005**, *10*, 1543−1550.
(42) Nobeli, I.; Laskowski, R. A.; Valdar, W. S.; Thornton, J. M. On the molecular discrimination between adenine and guanine by proteins. *Nucleic Acids Res.* **2001**, *29*, 4294−4309.

(43) Horecker, B. L.; Kornberg, A. The extinction coefficients of the reduced band of pyridine nucleotides. *J. Biol. Chem.* **1948**, *175*, 385−390.
(44) Siegel, J. M.; Montgomery, G. A.; Bock, R. M. Ultraviolet absorption spectra of DPN and analogs of DPN. *Arch. Biochem. Biophys.* **1959**, *82*, 288−299.
(45) Bock, R. M.; Ling, N. S.; Morell, S. A.; Lipton, S. H. Ultraviolet absorption spectra of adenosine-5′-triphosphate and related 5′-ribonucleotides. *Arch. Biochem. Biophys.* **1956**, *62*, 253−264.
(46) Liu, R.; Visscher, J. A novel preparation of nicotinamide mononucleotide. *Nucleosides Nucleotides* **1994**, *13*, 1215−1216.
(47) Leonidas, D. D.; Boix, E.; Prill, R.; Suzuki, M.; Turton, R.; Minson, K.; Swaminathan, G. J.; Youle, R. J.; Acharya, K. R. Mapping the ribonucleolytic active site of eosinophil-derived neurotoxin (EDN)—High-resolution crystal structures of EDN complexes with adenylic nucleotide inhibitors. *J. Biol. Chem.* **2001**, *276*, 15009−15017.
(48) Morrison, J. F.; Stone, S. R. Mechanism of the reaction catalyzed by dihydrofolate reductase from *Escherichia* coli: pH and deuterium isotope effects with NADPH as the variable substrate. *Biochemistry* **1988**, *27*, 5499−5506.
(49) Piotto, M.; Saudek, V.; Sklenar, V. Gradient-tailored excitation for single-quantum Nmr- spectroscopy of aqueous-solutions. *J. Biomol. NMR* **1992**, *2*, 661−665.
(50) Wiseman, T.; Williston, S.; Brandts, J. F.; Lin, L. N. Rapid measurement of binding constants and heats of binding using a new titration calorimeter. *Anal. Biochem.* **1989**, *179*, 131−137.

JM060490R